Supplement of Clim. Past, 16, 1325–1346, 2020
https://doi.org/10.5194/cp-16-1325-2020-supplement

Climate of the Past
Open Access
EGU

Supplement of

Greenland temperature and precipitation over the last 20 000 years using data assimilation

Jessica A. Badgeley et al.

Correspondence to: Jessica A. Badgeley (badgeley@uw.edu)

S1 Prior ensemble considerations

Here we elaborate on the pros and cons of four prior ensemble options we considered before deciding on the one that we use in this study (#4).

1. For offline data assimilation (i.e., no information passed between assimilation time steps), a justifiable method for choosing the prior ensemble would be to use a 100-member ensemble of 20,000-year climate simulations. These climate simulations would be TraCE-21ka-like (i.e., results from fully-coupled GCMs at T31 resolution or higher), and have varied initial conditions, boundary conditions, and model physics. The prior ensemble for any assimilation time step would be taken from the same time step in the climate simulations, which would lead to a prior ensemble that varies smoothly in time and is a justifiable initial guess for the climate evolution over the past 20,000 years. Though this option is simple, it is not feasible because the computational cost of running even one TraCE-21ka-like simulation remains near computational limits.

2. Given that there is only one TraCE-21ka-like simulation, another method would be to select states from TraCE-21ka that are closest in time to the reconstruction time step. For example, if we were reconstructing the 50-year average centered on the year 5,000 CE, then we would select the 100 states from TraCE-21ka that are closest in time to 5,000 CE. Given that we are working with 50-year averages, this means we would select all the states between 7,500 and 2,500 CE. This method, which we call the "running-window" method, provides a prior that varies smoothly in time and is a justifiable initial estimate for the climate evolution.

For the running-window method, the variance of the prior ensemble would tend to be small. A prior with small variance would lead to underweighting of the proxy records during assimilation. To avoid this issue, we could use the well-accepted approach of inflating the prior variance (Anderson and Anderson, 1999). However, the use of inflation adds an additional tunable parameter; in this case, it would add an additional parameter per time step. Although inflation can, in principle, be constrained using the ensemble calibration ratio (computed for excluded proxies), we have too few proxy records to meaningfully constrain this parameter without overfitting.

In addition to estimating numerous inflation factors, the running-window method limits us to one estimate of the spatial covariance structure per time step. Thus, we have no way to quantify the uncertainty associated with the prior covariance

structure. This could be fixed by expanding the running window and randomly selecting multiple prior ensembles; however, if the running window is expanded enough to create meaningfully different prior ensembles, then Holocene states will leak into glacial prior ensembles (and *vice versa*) and the method essentially becomes the method we use in the paper.

3. To reduce the number of inflation parameters, we could split TraCE-21ka into several distinct time periods. From these time periods, we would randomly select prior ensembles that are only used for the reconstruction of associated assimilation time steps. For example, if we split TraCE-21ka into glacial, transitional, and Holocene periods, then we'd make a glacial prior ensemble that is only used to reconstruct the glacial, a transitional prior ensemble that is only used to reconstruct the transition, and a Holocene prior ensemble that is only used to reconstruct the Holocene. This reduces the number of inflation factors we must estimate to a total of three. A disadvantage, however, is that this makes the prior discontinuous in time, which frequently leads to a discontinuous reconstruction. To adjust the reconstruction and make it continuous requires another source of information. Such post-processing adds an extra layer of complexity.

4. The method used in our study ensures a continuous reconstruction and removes the need for inflation factors. This method uses the same prior ensemble for all time steps (thus it is continuous) and the includes both glacial and Holocene states, which provides enough variance to appropriately weight the proxy records (thus no inflation is needed). Though the time-invariant prior is a poor estimate of the climate evolution over the last 20,000 years, the proxy records are given enough weight to result in a posterior that captures the large climate changes. In addition, we can quantify the uncertainty associated with the spatial covariance pattern by producing multiple posterior ensembles that each stem from a different prior ensemble. In the paper, we use ten different prior ensembles to quantify this uncertainty. Overall, this method is both feasible and simple, thus providing a first step in developing paleoclimate data assimilation for applications on glacial-interglacial timescales.

In this study, one state in a 100-member prior ensemble is an average over 50 years of the model data; these 100 states are selected randomly from the full length of the simulation. This implies that both glacial and Holocene states are likely to be contained within the same prior ensemble that is used to reconstruct all time steps over the last 20,000 years. A prior ensemble could in principle contain only Holocene states; however, this is not the case for any of the ten prior ensembles we use in the paper. Thus, in reconstructing a time step in the glacial, for example, both glacial and Holocene states are part of the prior ensemble.

S2 Accumulation records

Our aim is to develop simple, reproducible accumulation histories that are independent of temperature and water isotope assumptions and span the probable range of uncertainty. We use existing estimates for two sites (GISP2 and NEEM), but for three other sites (GRIP, NGRIP, and Dye3) we use one-dimensional ice-flow modeling to estimate the thinning function and convert measured layer-thickness into accumulation. Each core requires different ice-flow assumptions due to the different glaciological settings. Below we first describe the modeling approach used and then describe the reasoning for the ice-flow parameters chosen for each core.

S2.1 Model

We use a transient, one-dimensional, ice-flow model to calculate the cumulative vertical strain, termed the thinning function. We represent the vertical velocity profile using the Dansgaard and Johnsen (1969) formulation both because of its ubiquity in calculations of thinning for Greenland ice cores (Dahl-Jensen et al., 2003; Rasmussen et al., 2013; Dahl-Jensen et al., 1993) and it's simplicity:

$$w(z) = -(\dot{b} - \dot{m} - \dot{H})\psi(z) - \dot{m} \tag{1}$$

where z is the height above the bed in ice-equivalent meters (i.e. the firn has been compacted to ice), $\dot{b}$ is the accumulation rate, $\dot{m}$ is the melt rate, $\dot{H}$ is the rate of ice-thickness change, and $\psi(z)$ is the vertical velocity shape function computed as:

$$\psi(z) = \frac{f_B z + \frac{1}{2}(1 - f_B)\frac{z^2}{h}}{H - \frac{1}{2}h(1 - f_B)} \text{ for } h \geq z > 0 \tag{2}$$

$$\psi(z) = \frac{z - \frac{1}{2}h(1 - f_B)}{H - \frac{1}{2}h(1 - f_B)} \text{ for } H \geq z > h \tag{3}$$

following Dahl-Jensen et al. (2003) where h is the distance above bedrock of the Dansgaard and Johnsen (1969) kink height, f_B is the fraction of the horizontal surface velocity due to sliding over the bed, and H is the ice thickness. We assume no ice thickness change, $\dot{H} = 0$, and the f_B and $\dot{m}$ are constant in time with $\dot{b}(t)$ and $h(t)$ being functions of time.

The model is initially run with a constant accumulation history at the modern accumulation rate, and a thinning function is produced. The thinning function is then used with the measured layer thickness to infer a temporally-variable accumulation history. The model is then run with the temporally-variable accumulation history to produce an updated thinning function. This thinning function is then used with the measured layer thickness to infer the final accumulation history. The solution converges without additional iterations needed.

S2.2 NEEM

We use the accumulation reconstruction for the NEEM ice core from Rasmussen et al. (2013). Through the use of several different reconstruction methods, they developed a mean accumulation record with a two standard-deviation uncertainty envelope. We use their mean as our "moderate" record for the main reanalysis, the high end of their uncertainty envelope as our "high" estimate, and the low end of their uncertainty envelope as our "low" estimate.

S2.3 GISP2

The GISP2 ice core is located about 26 km from the ice divide at Summit, Greenland. The upper column of ice experiences vertical strain rates associated with flank flow, while ice close to the bed originated near the ice divide where vertical strain rates differ (Cuffey and Clow, 1997). The last 20,000 years of time is contained within the top two-thirds of the total ice thickness leading to a greater certainty in the vertical strain rates required to convert measured layer thickness into accumulation.

We use the accumulation reconstruction for the GISP2 ice core from Cuffey and Clow (1997) that coincides with their simulated 100 km retreat of the ice-sheet margin over the last 14,000 years. This reconstruction contains some uncertainty due to the vertical strain rates and margin-retreat scenario, but it is only weakly sensitive to changes in either one (Cuffey and Clow, 1997). Given these low uncertainties, we use this single accumulation record for our main, high, and low scenarios.

The Cuffey and Clow (1997) accumulation reconstruction is on an earlier depth-age scale (Alley et al., 1993; Meese et al., 1994; Bender et al., 1994). We transfer it onto the GICC05 depth-age scale by interpolating the GICC05 ages onto the accumulation depths and recalculating accumulation using:

$$A_{new} = A_{old}\frac{\lambda_{new}}{\lambda_{old}} \tag{4}$$

where A is accumulation, λ is the layer thickness, 'old' refers to the original depth-age scale from Cuffey and Clow (1997) and 'new' refers to the GICC05 depth-age scale. This approach accounts for errors in the depth-age scale while assuming the thinning function, with respect to depth, remains the same as the original record.

S2.4 GRIP

The GRIP ice core was drilled about 2 km from the true summit of Greenland. The basal temperature is well below freezing (Dahl-Jensen et al., 1998) and thus the melting term in the vertical velocity calculation can be neglected. Despite no Raymond arch being imaged with ice penetrating radar, phase sensitive radar (Gillet-Chaulet et al., 2011) revealed a vertical velocity profile influenced by the divide (i.e., the Raymond effect, Raymond, 1983). This indicates that the present divide position has not been stable long enough for a Raymond arch to develop (Marshall and Cuffey, 2000). The englacial vertical velocity profiles of Gillet-Chaulet et al. (2011) are not at the GRIP site and cannot directly inform our choice of profile. Because GRIP is not directly beneath the ice divide and the divide position has likely not been stable, we use a vertical velocity profile that is transitional between a typical flank profile and a divide profile; this is represented with a Dansgaard-Johnsen kink height of 0.4, which we use from 5 ka to present. Prior to 5 ka, we use a typically flank flow value of 0.1 assuming that the divide position is more than one ice thickness (3 km) away. The onset of divide flow at 5 ka is guided by 1) the inference of Vinther et al. (2009) of small surface elevation change around Greenland after 5 ka suggesting the ice sheet had reached a more stable configuration and 2) the duration of divide flow that could exist without a Raymond arch becoming visible. We use this as our moderate accumulation history and note that it is not sensitive to 1,000 year changes in the onset times of the divide flow.

The divide-like vertical velocity profiles causes more vertical strain near the surface of the ice sheet. Thus, an accumulation reconstruction that uses divide-like flow produces higher accumulation values. To develop the high and low scenarios, we use the divide-like kink height of 0.4 and the flank-like kink height of 0.1, respectively.

S2.5 NGRIP

The NGRIP ice-core site is located approximately 300 km north of GRIP along the central ridge of the Greenland Ice Sheet, where the high geothermal flux leads to a significant basal melt rate of approximately 7.7 mm a^{-1} (Dahl-Jensen et al., 2003). This melt rate should be included in the vertical velocity profile even though its primary influence is near the bed; the melting

also suggests the possibility that basal sliding contributes to the surface horizontal velocity. Dahl-Jensen et al. (2003) found an optimal fit to the depth-age relationship with the parameters $h = 0.45$, $f_B = 0.135$, $\dot{m} = 7.7$mm a^{-1}, and $\dot{b} = 0.19$ m a^{-1}. Gkinis et al. (2014) used the diffusion length of water isotopes to infer that these parameters produce too much thinning in the early Holocene, and suggested a linear correction of 25% less thinning to a depth of 2,000 m. A kink height of 0.45 is typically appropriate for ice-flow that is experiencing divide-like flow conditions. It would be unusual to have divide-like flow in a location with significant melt, as the Raymond effect is suppressed by basal sliding (Raymond, 1983; Pettit et al., 2003). We find that a kink-height of 0.2 reproduces the thinning function inferred by Gkinis et al. (2014) quite closely and is more easily interpreted dynamically because this value is expected for a site experiencing typical non-divide flow. The inverse method for inferring optimal model parameters as used by Dahl-Jensen et al. (2003) could be led astray by the assumption of direct scaling between accumulation and water isotopes.

For all scenarios, we use a melt rate of 7.7 mm a^{-1}. There may be small variations in the basal melt rate due to changes in the surface temperature and accumulation forcing and flow over bedrock with a different geothermal flux (Dahl-Jensen et al., 2003); however, any variations in the basal melt rate have a limited impact on the thinning inferred for the upper portion of the ice column. We use a kink height of 0.2 for our moderate scenario. For the high scenario, we use the original values of Dahl-Jensen et al. (2003). For the low scenario, we use a kink height of 0, which is equivalent to using a basal sliding fraction of 1, essentially the Nye model (Nye, 1963).

S2.6 Dye3

As discussed in the main text, reconstructing the accumulation rate at Dye3 is significantly more challenging than for the other interior ice-core sites. Ice of 20 ka age is much closer to the bed at Dye3 than at the central Greenland core locations, and has been strained to less than 10% of its original thickness. Complicating matters further, Dye3 was drilled at a site where the current surface velocity is 11 m yr^{-1}; the early Holocene ice has thus flowed many tens of kilometers (Whillans et al., 1984), possibly through significant accumulation variations (Reeh et al., 1985). Dye3 also has a more pronounced difference in ice fabric between the Holocene and glacial ice (Thorsteinsson et al., 1999; Montagnat et al., 2014). To develop the thinning function, we first compute the vertical velocity profile based on the horizontal strain measured with borehole tilt observations (Gundestrup and Hansen, 1984). These produced an accumulation history with an accumulation rate at the onset of the Holocene (11.7 ka) that is less than half of the modern accumulation rate. We consider this to be a low estimate, as the current velocity profile is strongly influenced by the location of the transition between the glacial and Holocene ice. We create a moderate scenario by approximately matching the accumulation rate around 7 ka with the past 1 ka accumulation rate; this uses a kink height of 0.2 which is typical for flank sites. We create a high scenario where we set the accumulation history at 11 ka approximately equal to the past 1 ka. The resulting accumulation histories vary significantly more than those for the interior cores because of the much greater uncertainty in the flow model.

We have not attempted to correct the accumulation history for advection because of the large uncertainties in both the flow path and the pattern of accumulation in the past. We note that we have low confidence in the Dye3 accumulation reconstructions; we include them because they are the only information from southern Greenland.

S3 Extension of the Dye3 depth-age scale to 20 ka

Here we explain the method we use to determine a Dye3 depth-age scale from 11.7 ka to 20 ka. Following the cross-correlation maximization procedure from Huybers and Wunsch (2004), we match the δ^{18}O record from Dye3 to the δ^{18}O record from NGRIP during this time interval. First we pick approximate tie points between the two δ^{18}O records. We emphasize placing tie points in the middle of high-magnitude, abrupt signals, such as the warming into the Bolling-Allerod, because these sigmals are most likely to be coherent across the ice sheet. Next we pick signals found in both δ^{18}O records regardless of magnitude and rate of change. We interpolate the depth-age scale between all the picked signals, including the tie points. We do this to achieve a close initial alignment of the two records, which gives us an initial correlation coefficient of 0.69 between the Dye3 and NGRIP δ^{18}O records. We then use the algorithm developed by Huybers and Wunsch (2004) to adjust the Dye3 depth-age scale to achieve a better alignment between these records. As input into the algorithm, we provide an age uncertainty estimate for each tie point and the amount of compression or extension each section between tie points is allowed to undergo. This latter constraint prevents both tie points from crossing and unrealistic changes in the implied accumulation rates. The updated depth-age scale output by this procedure gives a slightly higher correlation coefficient of 0.71.

S4 Importance of including a southern Greenland ice core

The Dye3 ice core is an important source of information for capturing southern Greenland climate. For example, we find that posterior ensemble mean compares quite well to independent (excluded) proxy records in central-northern Greenland, like NGRIP δ^{18}O; however, the equivalent for Dye3 shows a worse comparison, especially in the glacial (Fig. S1). This implies that the northern ice cores are uninformative for southern Greenland climate and/or the prior covariance structure does not properly convey information from northern ice cores to southern Greenland. The former demonstrates a need for data in southern Greenland, while the latter suggests a need for more climate-model simulations.

To evaluate whether each ice core is informative for southern Greenland climate, we compute the difference in evaluation metrics – correlation coefficient (Δ r), coefficient of efficiency (Δ CE), and root mean squared error (Δ RMSE) – between two sets of iterations when evaluated against Dye3, the only southern Greenland ice-core record. These two sets of iterations are: 1) ten iterations that exclude one proxy record, and 2) ten iterations that include all proxy records. We subtract the latter (all records) from the former (excluding one record), such that if the excluded proxy record is informative of southern Greenland climate, then the difference will be negative for r and CE and positive for RMSE.

To test the extent to which information from each core is spread to southern Greenland, we compute the change in ensemble variance (Δ variance) in southern Greenland for each set of iterations and average over time. To compute Δ variance, we divide by the iterations that include all proxy records, such that the result is fractional change in variance with a larger values indicating that more information is spread from the proxy record to southern Greenland. For this analysis, we focus on the change in variance for a region around Kangerlussuaq (65°N to 68.7°N and 48.5°W to 52.5°W), which does not overlap the location of Dye3.

We compute each "Δ" value as a mean over the Holocene to create a fair comparison between the proxy records that span different time periods; however, the implications of this analysis are insensitive to averaging over just the Holocene or the full 20,000 years.

Our reconstruction of southern Greenland temperature and precipitation generally improves with the inclusion of any of these ice-core records; however, it improves the most with the inclusion of the Dye3 records (Fig. S2). In addition, the Dye3 records result in the greatest change in ensemble variance in the Kangerlussuaq region (Fig. S2).

S5 Improvement of the reanalysis over the prior ensemble and TraCE-21ka

In Sect. 4.1, we present an evaluation of our main reanalysis using independent proxies and based on four skill metrics, correlation coefficient (r), coefficient of efficiency (CE), root mean square error (RMSE), and ensemble calibration ratio (ECR). Each of these skill metrics is described in detail in Sect. 2.3. We evaluate over three time periods, the full overlap of the reanalysis and the proxy record, a late-glacial period (20-15 ka), and period in the Holocene (8-3 ka). The computed skill metrics for the posterior ensemble are shown in Figs. 7 and 8. We compare these evaluation metrics to those of the prior ensemble (Figs. S6, and S7) and TraCE-21ka (Figs. S8 and S9). The skill metrics for TraCE-21ka are shown in Figs. S10 and S11.

S6 Methods for the O8, N3O5, and N3O5_BA experiments

The O8 experiment method differs from that for the main temperature reanalysis in the following way: it assimilates all eight δ^{18}O proxy records with the first 100-member prior ensemble, which results in just one iteration and a 100-member reanalysis ensemble.

The N3O5 experiment is similar to the O8 experiment except that it assimilates the three δ^{15}N-derived temperature records from Buizert et al. (2014) in place of the δ^{18}O records at the GIPS2, NEEM, and NGRIP sites. The temperature records are for the period 20 to 10 ka. To compute anomalies, we subtract site temperatures from the Box (2013) temperature reconstruction averaged over the reference period, 1850-2000 CE. To assimilate the δ^{15}N-derived temperature records we apply a direct-comparison proxy system model (PSM) (as is done for the main precipitation reanalysis) between the record and the simulated temperature at the model grid-cell closest to the ice-core site. For the δ^{15}N-derived temperature error variance, we use the reported variance values averaged across all time steps from the Buizert et al. (2014) supplementary information table. This gives error variance values of 6.35, 5.41, and 6.56 $^{\circ}C^2$ for the GISP2, NEEM, and NGRIP, records respectively.

The N3O5_BA experiment differs from the N3O5 experiment with respect to the prior ensemble. For the N3O5_BA experiment, we use a 100-member prior ensemble of 10-year averages (as opposed to 50-year averages) that is selected from the 1,000 years that surround the Bølling-Allerød warming (14.6 ka). This time period was selected to have a covariance pattern that shows greater variability at lower latitudes in Greenland, a pattern that is inferred from the δ^{15}N-derived temperature records (Guillevic et al., 2013; Buizert et al., 2014).

Figs. S12 and S13 show results from these three experiments for the warming out of the Younger Dryas and the warming into the Bølling-Allerød, respectively. The reconstructed climate-change patterns for these two events are nearly identical, but we show them both for completeness. The conclusions from these two events are qualitatively the same as those discussed in the main paper for the cooling into the Younger Dryas (Sect. 4.2, Fig. 12).

A comparison of results from our main reanalysis and Buizert et al. (2014) at each ice-core site can be found in Table S4 for each of the three abrupt temperature events.

References

Alley, R. B., Meese, D., Shuman, C., Gow, A., Taylor, K. C., Grootes, P., White, J., Ram, M., Waddington, E., Mayewski, P., et al.: Abrupt increase in Greenland snow accumulation at the end of the Younger Dryas event, Nature, 362, 527, 1993.

Anderson, J. L. and Anderson, S. L.: A Monte Carlo implementation of the nonlinear filtering problem to produce ensemble assimilations and forecasts, Monthly Weather Review, 127, 2741–2758, 1999.

Bender, M., Sowers, T., Dickson, M.-L., Orchardo, J., Grootes, P., Mayewski, P. A., and Meese, D. A.: Climate correlations between Greenland and Antarctica during the past 100,000 years, Nature, 372, 663, 1994.

Box, J. E.: Greenland ice sheet mass balance reconstruction. Part II: Surface mass balance (1840–2010), Journal of Climate, 26, 6974–6989, 2013.

Buizert, C., Gkinis, V., Severinghaus, J. P., He, F., Lecavalier, B. S., Kindler, P., Leuenberger, M., Carlson, A. E., Vinther, B., Masson-Delmotte, V., et al.: Greenland temperature response to climate forcing during the last deglaciation, Science, 345, 1177–1180, 2014.

Cuffey, K. M. and Clow, G. D.: Temperature, accumulation, and ice sheet elevation in central Greenland through the last deglacial transition, Journal of Geophysical Research: Oceans, 102, 26 383–26 396, 1997.

Dahl-Jensen, D., Johnsen, S., Hammer, C., Clausen, H., and Jouzel, J.: Past accumulation rates derived from observed annual layers in the GRIP ice core from Summit, Central Greenland, in: Ice in the climate system, pp. 517–532, Springer, 1993.

Dahl-Jensen, D., Mosegaard, K., Gundestrup, N., Clow, G. D., Johnsen, S. J., Hansen, A. W., and Balling, N.: Past temperatures directly from the Greenland ice sheet, Science, 282, 268–271, 1998.

Dahl-Jensen, D., Gundestrup, N., Gogineni, S. P., and Miller, H.: Basal melt at NorthGRIP modeled from borehole, ice-core and radio-echo sounder observations, Annals of Glaciology, 37, 207–212, 2003.

Dansgaard, W. and Johnsen, S.: A flow model and a time scale for the ice core from Camp Century, Greenland, Journal of Glaciology, 8, 215–223, 1969.

Gillet-Chaulet, F., Hindmarsh, R. C., Corr, H. F., King, E. C., and Jenkins, A.: In-situquantification of ice rheology and direct measurement of the Raymond Effect at Summit, Greenland using a phase-sensitive radar, Geophysical Research Letters, 38, 2011.

Gkinis, V., Simonsen, S. B., Buchardt, S. L., White, J., and Vinther, B. M.: Water isotope diffusion rates from the NorthGRIP ice core for the last 16,000 years–Glaciological and paleoclimatic implications, Earth and Planetary Science Letters, 405, 132–141, 2014.

Guillevic, M., Bazin, L., Landais, A., Kindler, P., Orsi, A., Masson-Delmotte, V., Blunier, T., Buchardt, S. L., Capron, E., Leuenberger, M., Martinerie, P., Prié, F., and Vinther, B. M.: Spatial gradients of temperature, accumulation and δ 18 O-ice in Greenland over a series of Dansgaard-Oeschger events., Climate of the Past, 9, https://doi.org/10.5194/cp-9-1029-2013, 2013.

Gundestrup, N. and Hansen, B. L.: Bore-hole survey at Dye 3, south Greenland, Journal of Glaciology, 30, 282–288, 1984.

Huybers, P. and Wunsch, C.: A depth-derived Pleistocene age model: Uncertainty estimates, sedimentation variability, and nonlinear climate change, Paleoceanography, 19, 2004.

Kindler, P., Guillevic, M., Baumgartner, M. F., Schwander, J., Landais, A., and Leuenberger, M.: Temperature reconstruction from 10 to 120 kyr b2k from the NGRIP ice core, Climate of the Past, 10, 887–902, 2014.

Marshall, S. J. and Cuffey, K. M.: Peregrinations of the Greenland Ice Sheet divide in the last glacial cycle: implications for central Greenland ice cores, Earth and Planetary Science Letters, 179, 73–90, 2000.

Meese, D. A., Gow, A., Grootes, P., Stuiver, M., Mayewski, P. A., Zielinski, G., Ram, M., Taylor, K., and Waddington, E.: The accumulation record from the GISP2 core as an indicator of climate change throughout the Holocene, Science, 266, 1680–1682, 1994.

Montagnat, M., Azuma, N., Dahl-Jensen, D., Eichler, J., Fujita, S., Gillet-Chaulet, F., Kipfstuhl, S., Samyn, D., Svensson, A., and Weikusat, I.: Fabric along the NEEM ice core, Greenland, and its comparison with GRIP and NGRIP ice cores, The Cryosphere, 8, 1129–1138, 2014.

Nye, J.: Correction factor for accumulation measured by the thickness of the annual layers in an ice sheet, Journal of Glaciology, 4, 785–788, 1963.

Pettit, E. C., Jacobson, H. P., and Waddington, E. D.: Effects of basal sliding on isochrones and flow near an ice divide, Annals of Glaciology, 37, 370–376, 2003.

Rasmussen, S. O., Abbott, P., Blunier, T., Bourne, A., Brook, E. J., Buchardt, S. L., Buizert, C., Chappellaz, J., Clausen, H. B., Cook, E., et al.: A first chronology for the North Greenland Eemian Ice Drilling (NEEM) ice core, Climate of the Past, 9, 2013.

Raymond, C. F.: Deformation in the vicinity of ice divides, Journal of Glaciology, 29, 357–373, 1983.

Reeh, N., Johnsen, S., Dahl-Jensen, D., Langway, C., Oeschger, H., and Dansgaard, W.: Dating the Dye 3 deep ice core by flow model calculations, Greenland ice core: geophysics, geochemistry and the environment, 33, 57–65, 1985.

Thorsteinsson, T., Waddington, E., Taylor, K., Alley, R. B., and Blankenship, D. D.: Strain-rate enhancement at Dye 3, Greenland, Journal of Glaciology, 45, 338–345, 1999.

Vinther, B. M., Buchardt, S. L., Clausen, H. B., Dahl-Jensen, D., Johnsen, S. J., Fisher, D., Koerner, R., Raynaud, D., Lipenkov, V., Andersen, K. K., et al.: Holocene thinning of the Greenland ice sheet, Nature, 461, 385, 2009.

Whillans, I. M., Jezek, K., Drew, A., and Gundestrup, N.: Ice flow leading to the deep core hole at Dye 3, Greenland, Annals of Glaciology, 5, 185–190, 1984.

Figures

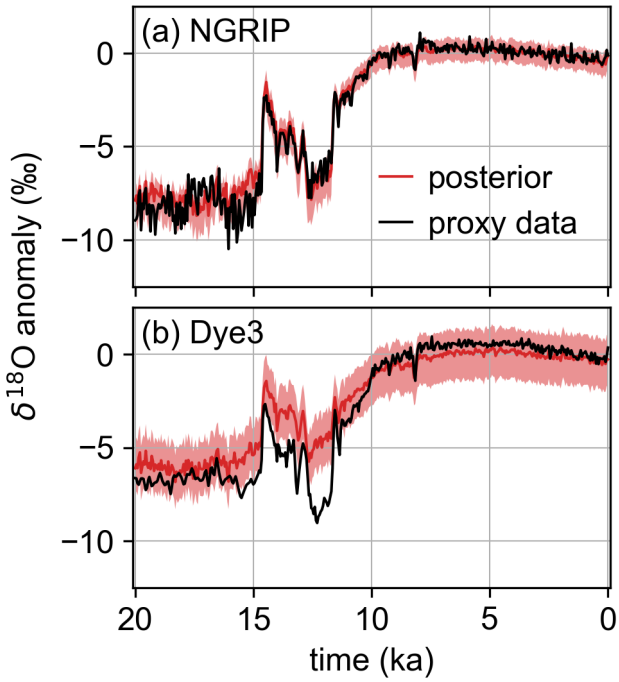

Figure S1. Comparison of the posterior (red) ensemble mean and 5^{th} to 95^{th} percentile shading to excluded proxy records (black) for (a) the NGRIP δ^{18}O record and (b) the Dye3 δ^{18}O record. We find that the proxy network is able to better capture northern-central proxy records like NGRIP than the southern Greenland record, Dye3, especially in the glacial period.

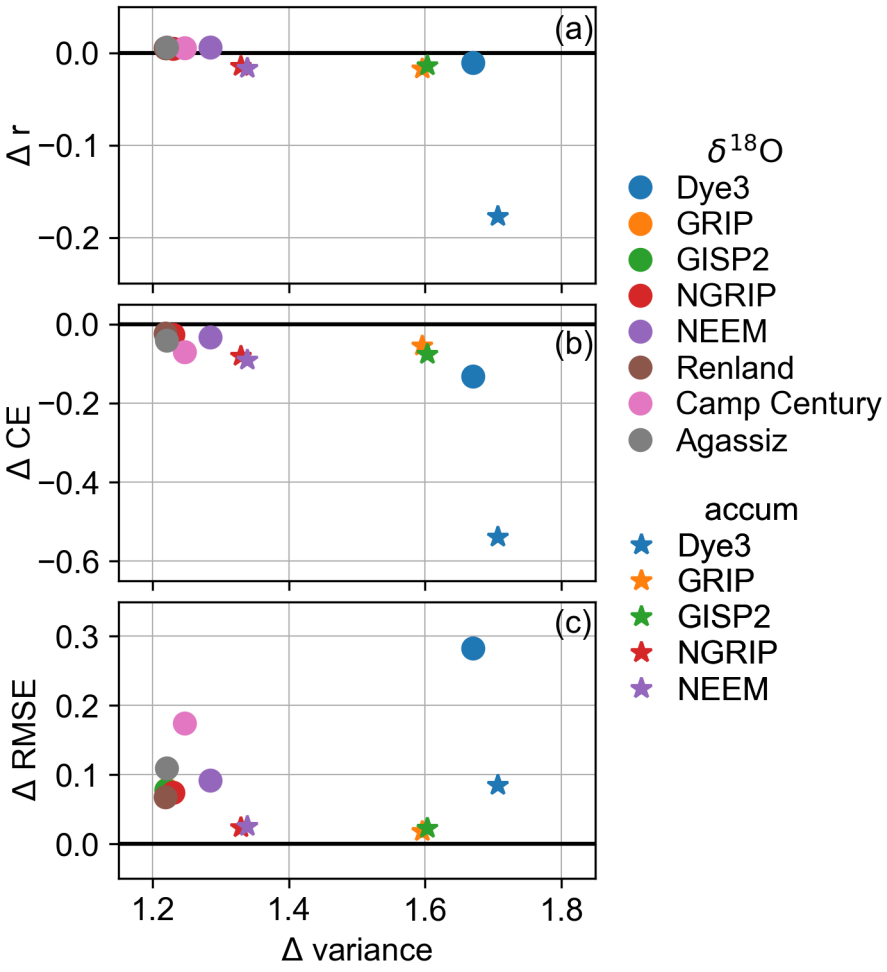

Figure S2. Relative importance of each ice-core record for reconstructing southern Greenland climate. On the absicissa is the change in posterior ensemble variance (Δ variance) in the Kangerlussuaq region, which indicates how much information is spread from a proxy record to that region. Higher values indicate more information has reached the region. On the ordinates are changes to skill metrics at the Dye3 ice-core site, which indicate whether proxy records are valuable for reconstructing southern Greenland climate. (a) shows results for the correlation coefficient (r), (b) shows results for the coefficient of efficiency (CE), and (c) shows results for the root mean square error (RMSE). Negative values of r and CE and positive values of RMSE indicate that the proxy record improves the reconstruction at the Dye3 site. The proxy record under consideration is indicated by colors (for the site) and symbols (for the proxy variable). Note that Δ RMSE values are in units of ‰ for δ^{18}O and are unitless for accumulation.

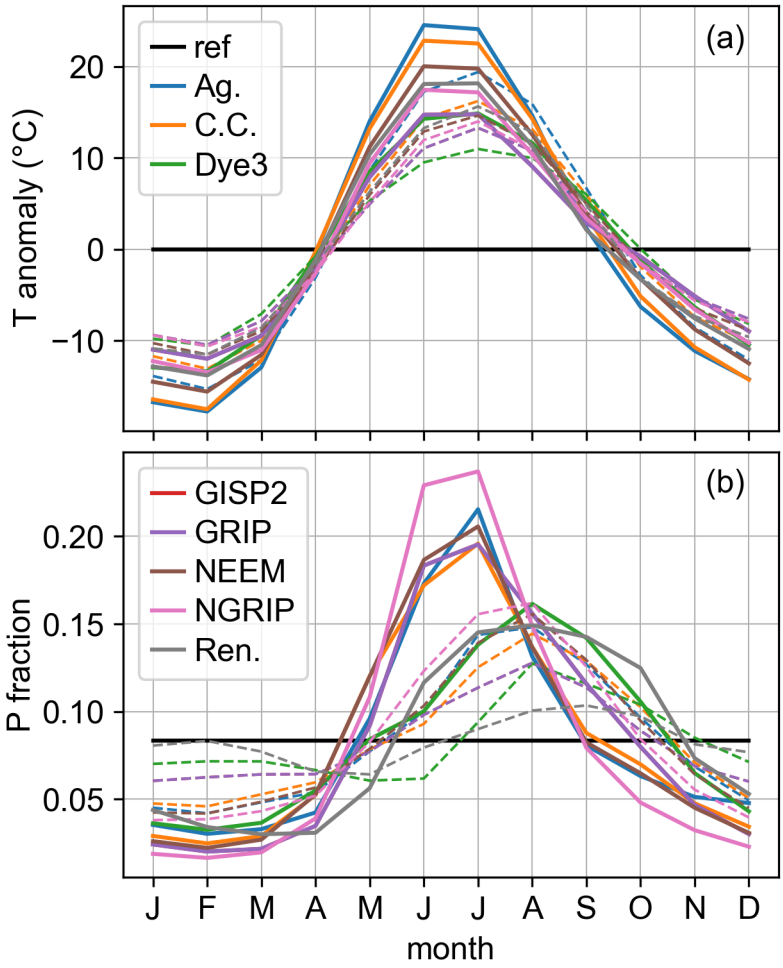

Figure S3. A comparison of TraCE-21ka glacial and Holocene seasonality at each ice-core site considered in this study. The mean glacial (20 to 15 ka) seasonality is shown as solid lines and the mean Holocene (5 to 0 ka) seasonality is shown as dashed lines. Panel (a) shows the monthly temperature anomaly referenced to the annual mean. Panel (b) shows the fraction of total annual temperature that fell each month. For both panels, the reference line (black) shows no seasonal cycle. Both the magnitude and the timing of the seasonal cycle change between the glacial and the Holocene, with the glacial generally showing a stronger seasonal cycle and an earlier summer peak. ref = reference line, Ag. = Agassiz, C.C. = Camp Century, and Ren. = Renland.

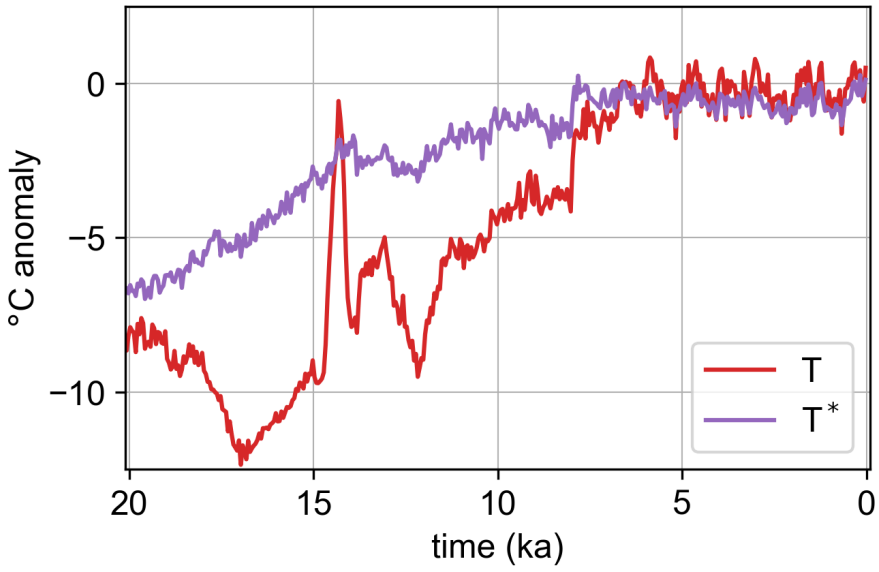

Figure S4. Temperature (T) and temperature weighted by monthly precipitation (T^*) from TraCE-21ka at Summit, Greenland. Both variables are shown as anomalies with respect to 1850-2000 CE and have been averaged to 50-year resolution. T^* was computed before the anomaly was taken.

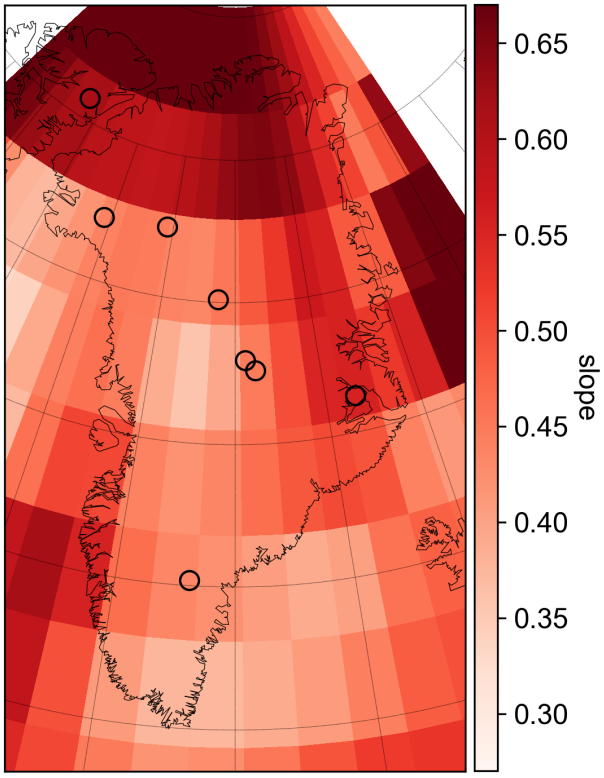

Figure S5. Slope (°C ‰$^{-1}$) of the linear δ^{18}O-temperature relationship for each grid cell of the prior ensemble. The δ^{18}O-temperature relationship between grid cells is not shown. This is an example from one of the prior ensembles. For reference, open circles show the locations of ice-core records used in this study.

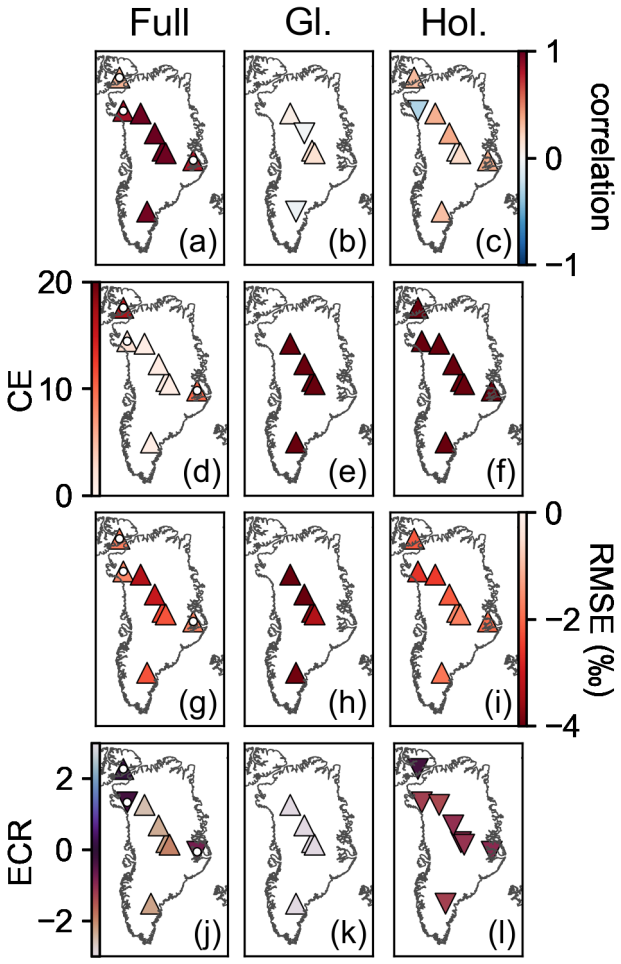

Figure S6. Change in skill metrics from the prior to posterior ensemble averaged over iterations and time for the temperature reanalysis. The first column (panels (a), (d), (g), and (j)) shows the skill-metric change for the full overlap (Full) between the proxy record and reanalysis. A white dot indicates evaluation against proxy records that overlap only the Holocene (11.7-0 ka). The middle column (panels (b), (e), (h), and (k)) shows the skill-metric change for a period in the glacial (Gl.) (20-15 ka), while the right column (panels (c), (f), (i), and (l)) is for a period in the Holocene (Hol.) (8-3 ka). The first row (panels (a)-(c)) reports the change in correlation coefficient, the second row (panels (d)-(f)) the coefficient of efficiency (CE), the third (panels (g)-(i)) the root mean square error (RMSE), and the fourth row (panels (j)-(l)) the ensemble calibration ratio (ECR). Triangle symbols pointing up indicate that the posterior ensemble evaluates better than the prior ensemble for that location and statistic. Triangle symbols pointing down indicate the opposite. We define better evaluation as correlation coefficient closer to 1, CE closer to 1, RMSE closer to 0, and ECR closer to 1.

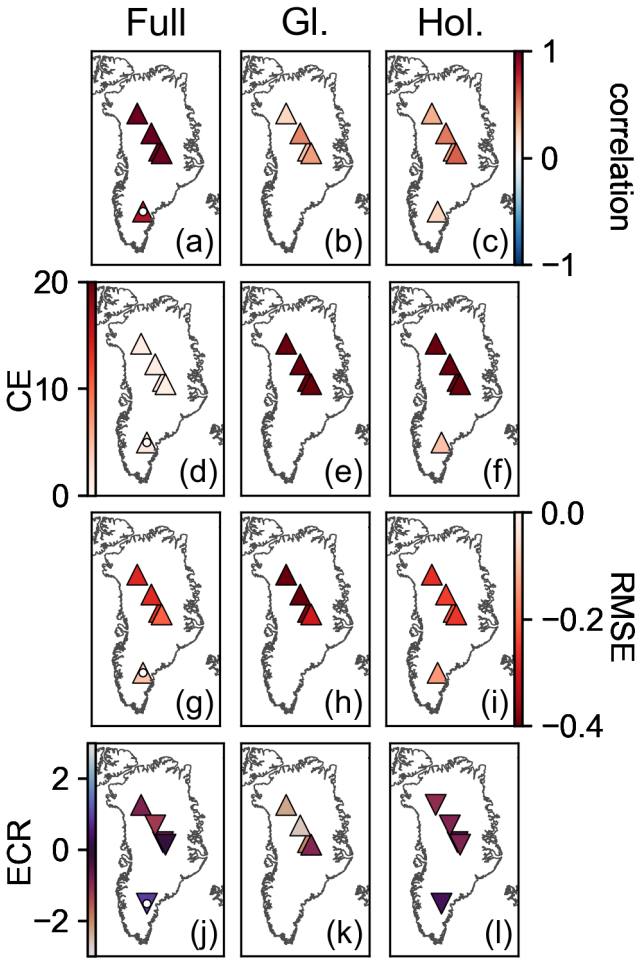

Figure S7. Change in skill metrics from the prior to posterior ensemble averaged over iterations and time for the precipitation reanalysis. The first column (panels (a), (d), (g), and (j)) shows the skill-metric change for the full overlap (Full) between the proxy record and reanalysis. A white dot indicates evaluation against proxy records that overlap only the Holocene (11.7-0 ka). The middle column (panels (b), (e), (h), and (k)) shows the skill-metric change for a period in the glacial (Gl.) (20-15 ka), while the right column (panels (c), (f), (i), and (l)) is for a period in the Holocene (Hol.) (8-3 ka). The first row (panels (a)-(c)) reports the change in correlation coefficient, the second row (panels (d)-(f)) the coefficient of efficiency (CE), the third (panels (g)-(i)) the root mean square error (RMSE), and the fourth row (panels (j)-(l)) the ensemble calibration ratio (ECR). Triangle symbols pointing up indicate that the posterior ensemble evaluates better than the prior ensemble for that location and statistic. Triangle symbols pointing down indicate the opposite. We define better evaluation as correlation coefficient closer to 1, CE closer to 1, RMSE closer to 0, and ECR closer to 1.

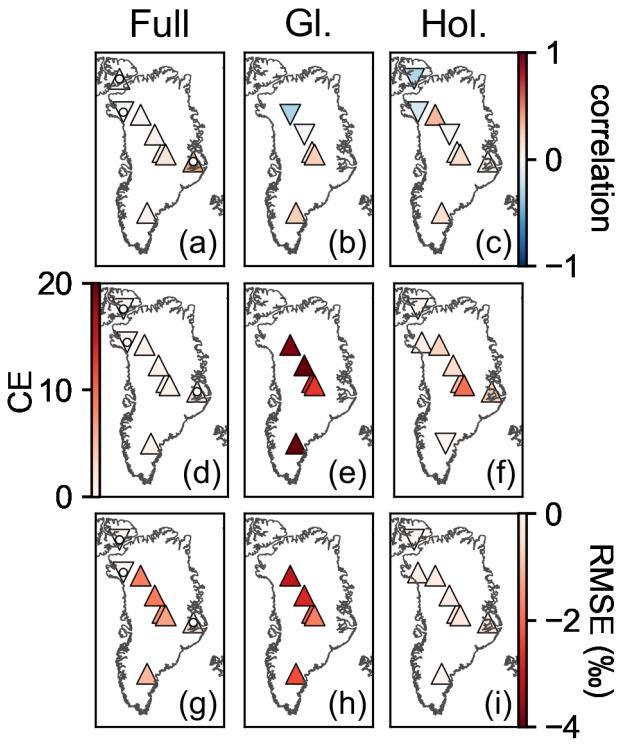

Figure S8. Change in skill metrics from TraCE-21ka to posterior ensemble averaged over iterations and time for the temperature reanalysis. The first column (panels (a), (d), (g), and (j)) shows the skill-metric change for the full overlap (Full) between the proxy record and reanalysis. A white dot indicates evaluation against proxy records that overlap only the Holocene (11.7-0 ka). The middle column (panels (b), (e), (h), and (k)) shows the skill-metric change for a period in the glacial (Gl.) (20-15 ka), while the right column (panels (c), (f), (i), and (l)) is for a period in the Holocene (Hol.) (8-3 ka). The first row (panels (a)-(c)) reports the change in correlation coefficient, the second row (panels (d)-(f)) the coefficient of efficiency (CE), the third (panels (g)-(i)) the root mean square error (RMSE), and the fourth row (panels (j)-(l)) the ensemble calibration ratio (ECR). Triangle symbols pointing up indicate that the posterior ensemble evaluates better than the prior ensemble for that location and statistic. Triangle symbols pointing down indicate the opposite. We define better evaluation as correlation coefficient closer to 1, CE closer to 1, RMSE closer to 0, and ECR closer to 1.

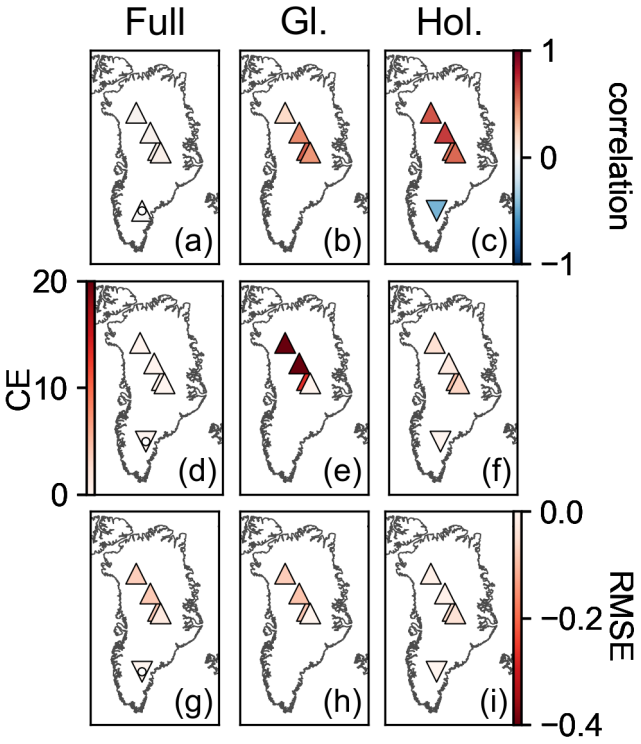

Figure S9. Change in skill metrics from TraCE-21ka to posterior ensemble averaged over iterations and time for the precipitation reanalysis. The first column (panels (a), (d), (g), and (j)) shows the skill-metric change for the full overlap (Full) between the proxy record and reanalysis. A white dot indicates evaluation against proxy records that overlap only the Holocene (11.7-0 ka). The middle column (panels (b), (e), (h), and (k)) shows the skill-metric change for a period in the glacial (Gl.) (20-15 ka), while the right column (panels (c), (f), (i), and (l)) is for a period in the Holocene (Hol.) (8-3 ka). The first row (panels (a)-(c)) reports the change in correlation coefficient, the second row (panels (d)-(f)) the coefficient of efficiency (CE), the third (panels (g)-(i)) the root mean square error (RMSE), and the fourth row (panels (j)-(l)) the ensemble calibration ratio (ECR). Triangle symbols pointing up indicate that the posterior ensemble evaluates better than the prior ensemble for that location and statistic. Triangle symbols pointing down indicate the opposite. We define better evaluation as correlation coefficient closer to 1, CE closer to 1, RMSE closer to 0, and ECR closer to 1.

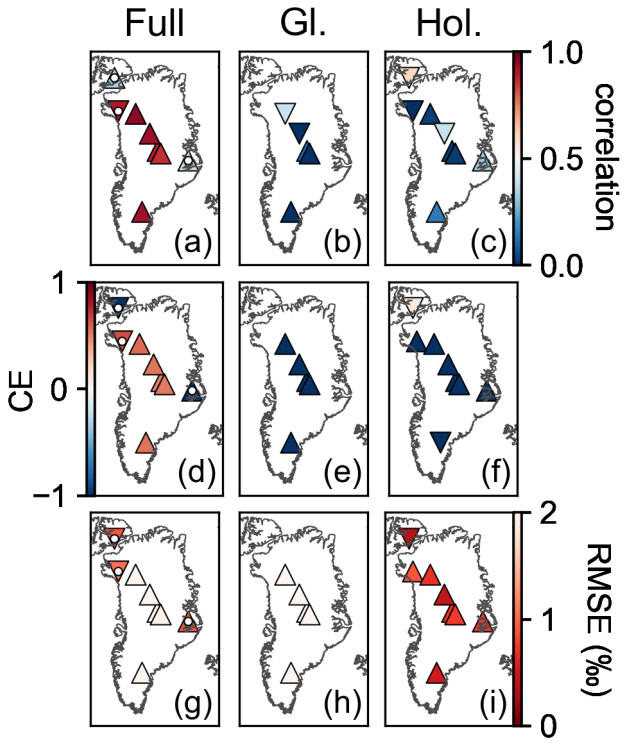

Figure S10. Temperature skill metrics for the TraCE-21ka simulation. The first column (panels (a), (d), (g), and (j)) shows the skill metrics for the full overlap (Full) between the proxy record and TraCE-21ka. A white dot indicates evaluation against proxy records that overlap only the Holocene (11.7-0 ka). The middle column (panels (b), (e), (h), and (k)) shows the skill metrics for a period in the glacial (Gl.) (20-15 ka), while the right column (panels (c), (f), (i), and (l)) is for a period in the Holocene (Hol.) (8-3 ka). The first row (panels (a)-(c)) reports the correlation coefficient, the second row (panels (d)-(f)) the coefficient of efficiency (CE), the third (panels (g)-(i)) the root mean square error (RMSE), and the fourth row (panels (j)-(l)) the ensemble calibration ratio (ECR). Triangle symbols pointing up indicate that the posterior ensemble of our main reanalysis evaluates better than TraCE-21ka for that location and statistic. Triangle symbols pointing down indicate the opposite. We define better evaluation as correlation coefficient closer to 1, CE closer to 1, RMSE closer to 0, and ECR closer to 1.

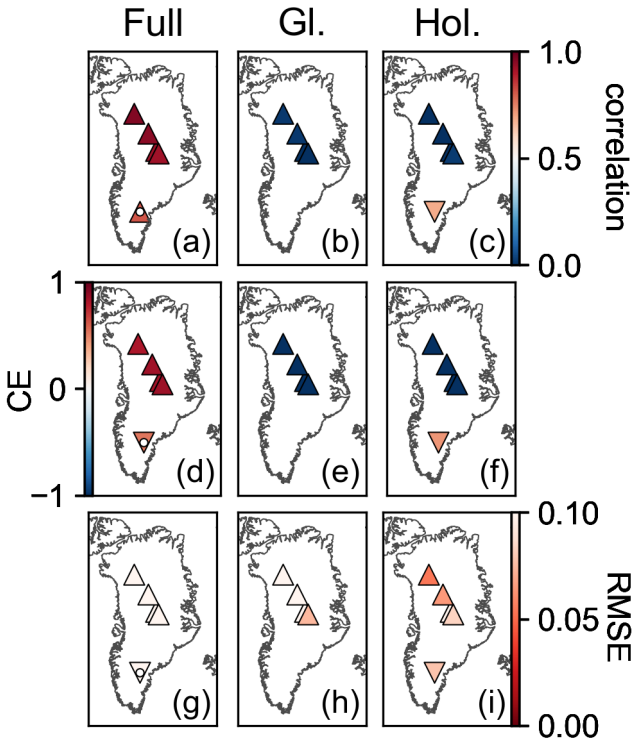

Figure S11. Precipitation skill metrics for the TraCE-21ka simulation. The first column (panels (a), (d), (g), and (j)) shows the skill metrics for the full overlap (Full) between the proxy record and TraCE-21ka. A white dot indicates evaluation against proxy records that overlap only the Holocene (11.7-0 ka). The middle column (panels (b), (e), (h), and (k)) shows the skill metrics for a period in the glacial (Gl.) (20-15 ka), while the right column (panels (c), (f), (i), and (l)) is for a period in the Holocene (Hol.) (8-3 ka). The first row (panels (a)-(c)) reports the correlation coefficient, the second row (panels (d)-(f)) the coefficient of efficiency (CE), the third (panels (g)-(i)) the root mean square error (RMSE), and the fourth row (panels (j)-(l)) the ensemble calibration ratio (ECR). Triangle symbols pointing up indicate that the posterior ensemble of our main reanalysis evaluates better than TraCE-21ka for that location and statistic. Triangle symbols pointing down indicate the opposite. We define better evaluation as correlation coefficient closer to 1, CE closer to 1, RMSE closer to 0, and ECR closer to 1.

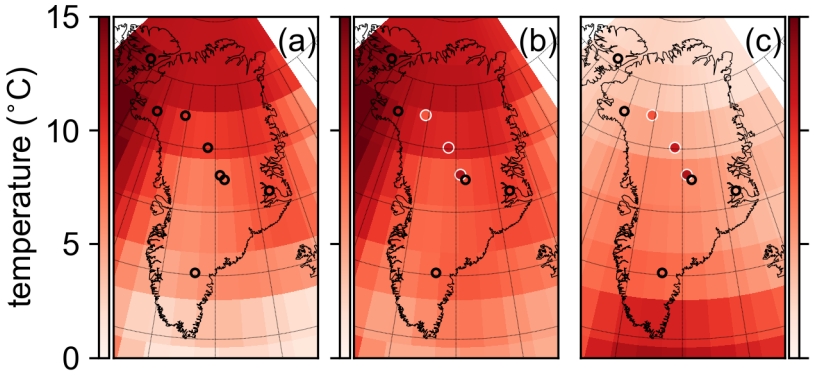

Figure S12. Spatial pattern of the abrupt warming event out of the Younger Dryas. Panel (a) shows results from experiment O8, assimilating all eight δ^{18}O records, panel (b) shows results from experiment N3O5, assimilating all three δ^{15}N-derived temperature records and the remaining five δ^{18}O records (those that do not overlap with the δ^{15}N sites), and panel (c) shows results from experiment N3O5_BA, which is similar to the N3O5 experiment except the prior ensemble is selected from the 1,000 years surrounding the Bølling-Allerød warming. Unfilled black circles show locations of assimilated δ^{18}O records, while filled circles with white outlines show locations of assimilated δ^{15}N-derived temperature records. Filled circles in panels (b) and (c) show the δ^{15}N-derived temperature values as reported by Buizert et al. (2014) on the same color scale as the rest of the panel. The temporal definition of this event is the same as defined in Buizert et al. (2014).

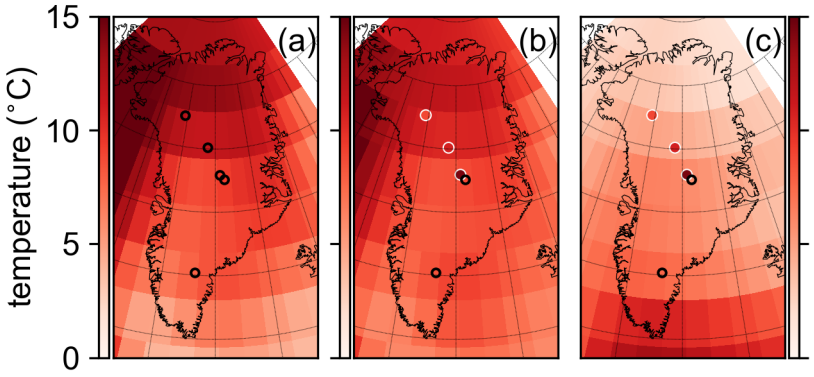

Figure S13. Spatial pattern of the abrupt warming event into the Bølling-Allerød. Panel (a) shows results from experiment O8, assimilating all eight δ^{18}O records, panel (b) shows results from experiment N3O5, assimilating all three δ^{15}N-derived temperature records and the remaining five δ^{18}O records (those that do not overlap with the δ^{15}N sites), and panel (c) shows results from experiment N3O5_BA, which is similar to the N3O5 experiment except the prior ensemble is selected from the 1,000 years surrounding the Bølling-Allerød warming. Unfilled black circles show locations of assimilated δ^{18}O records, while filled circles with white outlines show locations of assimilated δ^{15}N-derived temperature records. Filled circles in panels (b) and (c) show the δ^{15}N-derived temperature values as reported by Buizert et al. (2014) on the same color scale as the rest of the panel. The temporal definition of this event is the same as defined in Buizert et al. (2014).

Tables

Table S1. The mean slope for the linear δ^{18}O-temperature relationship used for the main reconstruction in this study (black, "main") and the mean slope for the relationship used in the S4 sensitivity experiment in this study (red, "S4"). We also include estimates from previous work, inlcuding, slopes found by Buizert et al. (2014) (purple, "B14") as seen in their Fig. 3 for five discontinuous time periods between 20 and 10 ka; slopes found by Guillevic et al. (2013) (green, "G13") from their Table 3 for Dansgaard-Oeschger events 8, 9, and 10; slopes found by Kindler et al. (2014) (blue, "K14") from their Fig. 5 and estimated from their Fig. 6 for 120 to 10 ka; and slopes found by Cuffey and Clow (1997) (orange, "C97") for time periods between 50 and 0.5 ka. The cores are arraged from North (top) to South (bottom).

Core Name	**Slope Range** ($^{\circ}$C ‰$^{-1}$)	**Slope Average** ($^{\circ}$C ‰$^{-1}$)
Agassiz	main: 0.618 - 0.656	0.640
	S4: 0.412 - 0.437	0.425
Camp Century	main: 0.439 - 0.468	0.456
	S4: 0.293 - 0.312	0.304
NEEM	main: 0.450 - 0.480	0.465
	S4: 0.300 - 0.320	0.310
	B14: 0.25 - 0.76	0.50
	G13: 0.51 - 0.63	0.57
NGRIP	main: 0.454 - 0.489	0.470
	S4: 0.303 - 0.326	0.313
	B14: 0.29 - 0.41	0.36
	G13: 0.34 - 0.47	0.42
	K14: 0.3 - 0.57	0.52
GISP2	main: 0.442 - 0.493	0.467
	S4: 0.294 - 0.329	0.311
	B14: 0.11 - 0.30	0.25
	G13: 0.38	
	C97: 0.251 - 0.465	0.324
GRIP	main: 0.442 - 0.493	0.467
	S4: 0.294 - 0.329	0.311
	G13: 0.49	
Renland	main: 0.546 - 0.595	0.571
	S4: 0.364 - 0.397	0.381
Dye3	main: 0.424 - 0.475	0.444
	S4: 0.283 - 0.317	0.296

Table S2. Comparison of abrupt climate transitions in our main reconstruction and sensitivity reconstructions, S1, S2, S3, and S4. We use the same time definitions as in Buizert et al. (2014). Note that the main reconstruction and S4 do not warm as rapidly out of the Younger Dryas as S1, S2, and S3. Thus, our use of a single time definition may not allow us capture the full transition for all of these reconstructions.

Core Name	Reconstruction Name	Bølling-Allerød warming	Younger Dryas cooling	Younger Dryas warming
Agassiz	Main (δ^{18}O$= 0.67T^*$)	12.83	-9.10	11.64
	S1 (δ^{18}O$= 0.67T$)	8.67	-5.16	7.78
	S2 (δ^{18}O$= 0.5T$)	11.20	-6.96	10.50
	S3 (δ^{18}O$= 0.335T$)	15.41	-9.99	14.84
	S4 (δ^{18}O$= 0.67T^*$, stronger P seasonality)	15.49	-11.05	13.06
Camp Century	Main	11.71	-8.51	10.53
	S1	8.04	-4.94	7.13
	S2	10.40	-6.60	9.65
	S3	14.34	-9.41	13.71
	S4	14.07	-10.36	11.46
NEEM	Main	10.17	-7.53	9.10
	S1	7.11	-4.51	6.34
	S2	9.22	-5.99	8.33
	S3	12.74	-8.47	12.16
	S4	12.18	-9.20	9.71
NGRIP	Main	9.62	-7.17	8.57
	S1	6.76	-4.33	6.03
	S2	8.77	-5.73	8.14
	S3	12.13	-8.09	11.57
	S4	11.52	-8.77	9.07
GISP2	Main	7.78	-6.03	6.88
	S1	5.66	-3.88	5.18
	S2	7.39	-5.06	6.92
	S3	10.26	-7.03	9.81
	S4	9.27	-7.41	7.03
GRIP	Main	7.78	-6.03	6.88
	S1	5.66	-3.88	5.18
	S2	7.39	-5.06	6.92
	S3	10.26	-7.03	9.81
	S4	9.27	-7.41	7.03
Renland	Main	8.51	-6.27	7.77
	S1	5.93	-3.78	5.39
	S2	7.70	-5.02	7.22
	S3	10.64	-7.08	10.22
	S4	10.15	-7.62	8.53
Dye3	Main	6.45	-5.64	5.41
	S1	5.33	-4.34	5.26
	S2	7.05	-5.45	6.84
	S3	9.92	-7.29	9.60
	S4	7.62	-7.10	4.79

Table S3. Scaling factors (β) for the temperature-precipitation relationship in the Kangerlussuaq region. The results for the main reanalysis are in bold.

Temperature scenario	**Precipitation scenario**	**No Filtering**	**Low-Pass (5,000 years^{-1})**	**High-Pass (5,000 years^{-1})**
Main	Low	0.09	0.09	0.04
Main	**Moderate**	**0.08**	**0.08**	**0.04**
Main	High	0.08	0.08	0.05
S1	Low	0.12	0.11	0.05
S1	Moderate	0.11	0.11	0.06
S1	High	0.11	0.11	0.07
S2	Low	0.09	0.09	0.04
S2	Moderate	0.09	0.08	0.04
S2	High	0.09	0.08	0.05
S3	Low	0.06	0.06	0.03
S3	Moderate	0.06	0.06	0.03
S3	High	0.06	0.06	0.04
S4	Low	0.07	0.07	0.03
S4	Moderate	0.07	0.07	0.03
S4	High	0.07	0.07	0.04

Table S4. Comparison of abrupt climate transitions in our main reconstruction (black) and from Buizert et al. (2014) (purple values in the second row for NEEM, NGRIP, and GISP2). Uncertainties are given as standard deviations. We use the published values and uncertainties from Buizert et al. (2014). We use the same time definitions as in Buizert et al. (2014).

Core Name	**Bølling-Allerød warming**	**Younger Dryas cooling**	**Younger Dryas warming**
Agassiz	12.83 ± 3.49	-9.10 ± 3.65	11.64 ± 3.46
Camp Century	11.71 ± 3.23	-8.51 ± 3.42	10.53 ± 3.24
NEEM	10.17 ± 3.01 8.9 ± 1.2	-7.53 ± 3.2 -4.8 ± 0.6	9.10 ± 3.05 8.4 ± 1.5
NGRIP	9.62 ± 2.90 10.8 ± 1.0	-7.17 ± 3.09 -10.9 ± 1.0	8.57 ± 2.95 11.4 ± 1.6
GISP2	7.78 ± 2.77 14.4 ± 0.95	-6.03 ± 2.96 -9.2 ± 0.45	6.88 ± 2.84 12.4 ± 1.7
GRIP	7.78 ± 2.77	-6.03 ± 2.96	6.88 ± 2.84
Renland	8.51 ± 2.55	-6.27 ± 2.70	7.77 ± 2.57
Dye3	6.45 ± 3.84	-5.64 ± 4.10	5.41 ± 3.96